IEEE Access
Multidisciplinary ⋮ Rapid Review ⋮ Open Access Journal

Received 9 August 2023, accepted 16 August 2023, date of publication 21 August 2023, date of current version 29 August 2023.

Digital Object Identifier 10.1109/ACCESS.2023.3307186

RESEARCH ARTICLE

Comparative Characterization of Indoor VLC and MMW Communications via Ray Tracing Simulations

FAHIMEH AGHAEI[1], (Student Member, IEEE), HOSSIEN B. ELDEEB[2], (Senior Member, IEEE), LINA BARIAH[2,3], (Senior Member, IEEE), SAMI MUHAIDAT[2], (Senior Member, IEEE), AND MURAT UYSAL[4], (Fellow, IEEE)

[1]Department of Electrical and Electronics Engineering, Özyeğin University, Istanbul 34794, Turkey
[2]Center for Cyber-Physical Systems, Department of Electrical Engineering and Computer Science, Khalifa University, Abu Dhabi, United Arab Emirates
[3]Technology Innovation Institute, Abu Dhabi, United Arab Emirates
[4]Engineering Division, New York University Abu Dhabi (NYUAD), Abu Dhabi, United Arab Emirates

Corresponding authors: Hossien B. Eldeeb (hossien.eldeeb@ku.ac.ae) and Fahimeh Aghaei (fahimeh.aghaei@ozu.edu.tr)

ABSTRACT The demand for ultra-high-speed indoor wireless connectivity is ever-increasing, which poses unique challenges for the next generation wireless communication system design. This has prompted the exploration of higher frequency bands including millimeter wave (MMW) and visible light bands in addition to the conventional sub-6 GHz band. This paper provides a comprehensive comparison of the propagation channels of these frequency bands under the same indoor environment and scenarios. We adopt ray tracing techniques for site-specific channel modeling, which enables the consideration of the three-dimensional models of the indoor environment and objects inside. It allows us to take into account different frequencies, i.e., 2.4 GHz, 6 GHz, 28 GHz, 60 GHz, 100 GHz, and visible light band as well as different transmitter types, i.e., omnidirectional/directional antennas for radio frequency systems and indoor luminaries for visible light communications (VLC). For different frequencies under consideration, we obtain channel impulse responses (CIRs) and present the channel path losses for various user trajectories in indoor environments. Furthermore, we propose closed-form expressions for the cumulative distribution functions (CDFs) of received power levels for all frequency bands under consideration. Our results demonstrate that VLC channels exhibit lower path loss than that in MMW bands but higher than that of 2.4 GHz band. In addition, it is observed that VLC systems exhibit more sensitivity to shadowing and blockage effects. Our findings further indicate that the characteristics of the propagation channel are greatly influenced by the antenna type. For instance, using omnidirectional and rectangular patch antennas results in lower path loss compared to horn antennas, and this difference becomes more significant as the transmission distance decreases.

INDEX TERMS Radio frequency (RF), visible light communication (VLC), hybrid RF/VLC, wireless fidelity (Wi-Fi), hybrid networks, hybrid RF/VLC environments.

I. INTRODUCTION

More than 70 % of wireless voice and data traffic take place in an indoor environment [1], [2]. Low-cost and high-data-rate solutions are required to enable ubiquitous indoor wireless connectivity as well as avoid making congestion in the radio frequency (RF) spectrum. The omnipresence of Light Emitting Diodes (LEDs) in indoor environments provides a unique opportunity for visible light communication (VLC) to exploit the existing illumination infrastructure for wireless access [3], [4], [5]. VLC has therefore emerged as a complementary solution to RF-based wireless systems [6], [7], [8], [9]. While the millimetre-wave (MMW) and visible light are different in nature, they exhibit some similarities due to operating at higher frequencies compared to sub-6 GHz systems [10], [11]. It is therefore

The associate editor coordinating the review of this manuscript and approving it for publication was Tutku Karacolak.

This work is licensed under a Creative Commons Attribution-NonCommercial-NoDerivatives 4.0 License.
For more information, see https://creativecommons.org/licenses/by-nc-nd/4.0/

critical to explore the fundamental characteristics of these two technologies.

Several works have already investigated RF channel modeling for indoor scenarios [12], [13], [14], [15], [16], [17]. For example, the works in [12], [13], [14], and [15] examined the RF propagation channels at low-frequency bands of 2.4 GHz [12], 10 GHz [13], 11 GHz [14], and 23.5 GHz [15]. Although [12] and [13] assumed the availability of the direct Line-of-Sight (LOS) link, [14] and [15] considered the case of obstructed LOS called Non-LOS (NLOS) and its effect. The impact of the higher MMW frequencies up to 60 GHz on indoor channels was then examined in [16] and [18]. The wide-band channel measurements were also conducted in [17] to investigate the effect of propagation distance on indoor scenarios.

Indoor VLC channel modeling was also examined in some studies [19], [20], [21], [22], [23], [24]. In [19], the commonly used Lambertian channel model with a LOS link was considered to analyze the indoor VLC channel delay factors. Then, the authors in [20] and [21] modified that model to investigate the impact of shadowing (due to obstacles) [20] and the multipath reflections [21] on the indoor VLC channels. In [22] and [23], based on an advanced non-sequential ray-tracing approach, the channel impulse responses (CIRs) were obtained for different indoor VLC scenarios considering the impact of surface reflectance and a large number of reflections for better accuracy. Experimental measurements were also conducted to study the indoor VLC channel characteristics [24] and/or validate the ray tracing results [25], i.e., see [26] and references therein.

Most of the earlier works focus on individual technology and do not present a one-to-one comparison of indoor MMW and VLC channels. To the best of our knowledge, the only prior works that attempt to make such a comparison are [27], [28]. The work in [27] compared the channel modeling of both the VLC and MMW systems in an empty room based on a simple path loss model. The path loss and time dispersion were calculated for both MMW and VLC assuming different antenna gains for 28, 60, and 73 GHz and VLC bands. The work in [28] used a ray tracing tool to compare the channel characteristics of VLC/RF indoor systems assuming 7 hexagonal micro-cells.

In this paper, we compare the propagation channels of RF and VLC spectra for the same indoor environment and scenarios. Several RF frequencies are considered, including 2.4 GHz, 6 GHz, 28 GHz, 60 GHz, 100 GHz. We benefit from the advanced features of the ray-tracing methodology for modeling both the VLC and RF propagation channels. We take into account the realistic models of the indoor environment, the objects inside, and the typical antenna radiation patterns. Taking into account the impact of the LOS, reflected, refracted, and scattered rays, we investigate the channel characteristics for different user positions, receiver locations, and user trajectories (i.e., diagonal, vertical, and horizontal paths). We analyze the results of CIRs and the channel path loss for different positions of users, frequencies, locations of receivers, and antenna types. The obtained results demonstrate that the propagation channel characteristics are highly dependent on the antenna type as well as the geometry of the user and the receiver's location.

TABLE 1. List of notations used in this paper.

Notation	Definition
$h_{\mathbf{MMW}}(t)$	MMW channel impulse response
N_P	Number of RF emitted rays
A_i	Amplitude of i^{th} ray
ψ_i	Phase of i^{th} ray
$PL_{\mathbf{MMW}}$	MMW channel path loss
P_{ijk}	Power of i^{th} ray emitted from the j^{th} transmitter and reached the k^{th} PD
τ_{ijk}	Propagation delay of i^{th} ray emitted from the j^{th} transmitter and reached the k^{th} PD
N	Number of VLC emitted rays
M	Number of luminaires/VLC transmitters
$h_k\,(t)$	VLC channel impulse response at the k^{th} PD
$\delta\,(t)$	Dirac delta function
$P_{t,\mathbf{opt}}$	Transmit optical power
$P_{r,\mathbf{opt},k}$	Received optical power at the k^{th} PD
$P_{r,k}$	Received electrical power at the k^{th} PD
P_t	Transmit electrical power
H_k	VLC DC channel gain at the k^{th} PD
R_L	Load to the photo detector
G_A	Trans-Impedance gain
$PL_{\mathbf{VLC},k}$	VLC channel path loss at the k^{th} PD
ε_r	Relative permittivity
σ	Relative conductivity
PX	Position of Xth cell in the room
T_u	u^{th} trajectory of the user
$\Re$	Responsivity of the PD
η	Electrical-to-optical conversion ratio

The rest of the paper is organized as follows: In Section II, we describe channel modeling methodology. In Section III, we describe the indoor scenarios under consideration. Section IV provides simulation results and discussions. Finally, conclusions are drawn in Section V.

II. CHANNEL MODELING METHODOLOGY

In this paper, we use Remcom's Wireless Insite [29] and Zemax's OpticStudio® [30] software tools respectively for RF and VLC channel modeling. To have a precise characterization of the signal interaction with the environment, these simulators build upon advanced non-sequential ray tracing features to enable integration of the realistic source radiation patterns and wavelength-dependent reflectance of the surface coating. It can be noted that the channel models obtained by the considered ray tracing methods have been validated by real measurement/empirical data [31], [32], [33], [34]. For instance, for the VLC system in [34], the channel impulse and frequency responses were measured using a frequency sweeping technique at different indoor scenarios. Results of both the measurement and the considered ray tracing method have indicated a very good match validating the ray tracing method. On the other hand, for MMW, the authors in [31] demonstrated through experimental validation at 100-300 GHz that the ray tracing method is an effective and highly accurate channel modeling approach for MMW and THz channels. Table 1 summarizes the notations that will be used in the rest of the paper.

A. RF CHANNEL MODELING

Ray tracing is a classical deterministic method for analyzing site-specific radio wave propagation. It builds upon the geometrical optic and uniform theory of diffraction to model the interactions between the rays and objects, including the reflection from various surfaces, transmission via indoor objects, scattering, and diffraction from edges.

In the following, we describe the main steps in our simulation study. First, we create a three-dimensional (3D) model of the indoor environment in the Wireless Insite where the CAD models of a human and a cell phone are imported, see Fig.1.a. Then, the transmitter (TX) and receiver (RX) specifications including antenna type, radiation pattern, orientation, etc are defined. Maximum gain, polarization, aperture/feed width and height, and feed-aperture length are additional inputs related to antenna type characterization. In the simulations, rays originating from the transmitter encounter objects (i.e., indoor surfaces, the human body, etc.), and the losses in the strength of the propagating signal depend on the electrical features of the surface materials. The frequency dependence of surface materials in terms of permittivity, conductivity, and thickness [35] to characterize these interactions are further taken into account. For example, the reflections of the walls, floor, and ceiling are characterized as a mix of specular and diffuse in our study while the reflections of the cellphone with metal material are modeled as specular [36]. The reflection type in materials can be determined by the ''scatter fraction'' parameter in the X3D propagation model of Wireless Insite. This parameter varies between 0 and 1 such that zero indicates the purely specular reflections and unity notes the purely diffuse case.

The Shoot-and-Bounce Ray (SBR) method is used in Wireless Insite [37] to obtain the CIR. The rays are launched with angular spacing and traced back to the RXs. The CIR consists of LOS rays as well as n^{th}- order NLOS rays related to the floor, ceiling, walls, and objects. Wireless Insite can generate specific outputs such as received power, path loss, and CIR automatically by selecting those items in the output window. The CIR is given by

$$h_{\text{MMW}}(t) = \sum_{i=1}^{N_p} A_i \exp\left(j\psi_i\right)\delta\left(t-\tau_i\right), \tag{1}$$

where N_P is the number of paths and τ_i is the delay of the i^{th} path. A_i and ψ_i are respectively the amplitude (in voltage) and phase of the channel coefficient associated with the i^{th} path. They are defined as

$$A_i = E_{\theta,i}g_\theta(\theta_i,\phi_i) + E_{\phi,i}g_\theta(\theta_i,\phi_i), \tag{2}$$

$$\psi_i = \tan^{-1}\left(\frac{\text{Im}\left(A_i\right)}{\text{Re}\left(A_i\right)}\right), \tag{3}$$

where $E_{\theta,i}$ and $E_{\phi,i}$ are the so-called theta and phi components of the electric field of the i^{th} path at the receiver point while θ_i and ϕ_i are the parameters related to the direction of arrival ray. $g_\theta(\theta_i,\phi_i)$ indicates the direction of arrival angles including the elevation and azimuth angles. The channel path loss (in linear scale), including the effect of antenna gains, is calculated by

$$PL_{\text{MMW}} = \left(\frac{\lambda^2\beta}{8\pi\eta_0}\right)\left|\sum_{i=1}^{N_P} E_{\theta,i}g_\theta(\theta_i,\phi_i) + E_{\phi,i}g_\phi(\theta_i,\phi_i)\right|^2, \tag{4}$$

where λ is the wavelength and η_0 is the impedance of free space (377 Ω). The quantity β is the overlap of the frequency spectrum of the transmitted waveform and the spectrum of the frequency sensitivity of the receiver.

B. VLC CHANNEL MODELING

For VLC channel modeling, we utilize the non-sequential ray-tracing approach in [22] and [36] which has been recently validated in [34]. In this method, a 3D simulation platform with CAD models is constructed in OpticStudio® software (See Fig. 1b). To precisely capture the interaction of the rays with the indoor environment and objects inside, we specify the optical characteristics of the room surface coating by defining their wavelength-dependent reflectance values utilizing the built-in function ''Table Coating'' provided by OpticStudio® tools. For TX modeling in the simulation platform, we first create the photometric data (i.e., IES file) of the lighting source under investigation which contains the luminous intensity in all different planes. The photometric file is imported into the software along with the spectral power distribution of the luminaries. Then, we define the other light sources specifications such as spectral bandwidth, optical power, and orientations. Similarly, the RX specifications such as orientations, field-of-view (FoV) angle, and aperture diameter are defined.

After the simulation platform is constructed, we run non-sequential OpticStudio®. The output includes the received power and the path length information for each ray that is emitted from the light source and reaches the detector. These are then imported into MATLAB to construct optical CIR. Let P_{ijk} and τ_{ijk} respectively denote the optical power and the propagation delay of the i^{th} ray, i=1,2,…,N, which is emitted from the j^{th} luminaire, j=1,2,…,M, and reaches the k^{th} Photo-Detector (PD). The optical CIR at the k^{th} PD is therefore written as

$$h_k(t) = \sum_{j=1}^{N}\sum_{i=1}^{M} P_{ijk}\delta\left(t-\tau_{ijk}\right), \tag{5}$$

where $\delta(t)$ is the Dirac delta function. For a given transmit optical power of $P_{t,\text{opt}}$, the received optical power at the k^{th} PD is calculated by

$$P_{r,\text{opt},k} = P_{t,\text{opt}}H_k = P_{t,\text{opt}}\int_0^\infty h_k(t)\,dt, \tag{6}$$

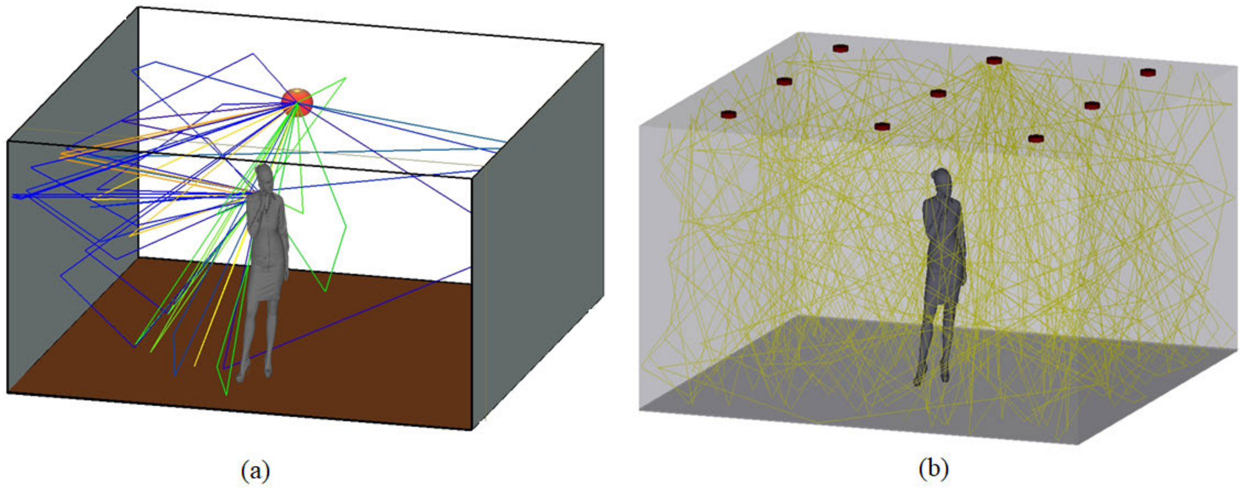

FIGURE 1. Modeling layout for (a) RF system and (b) VLC system.

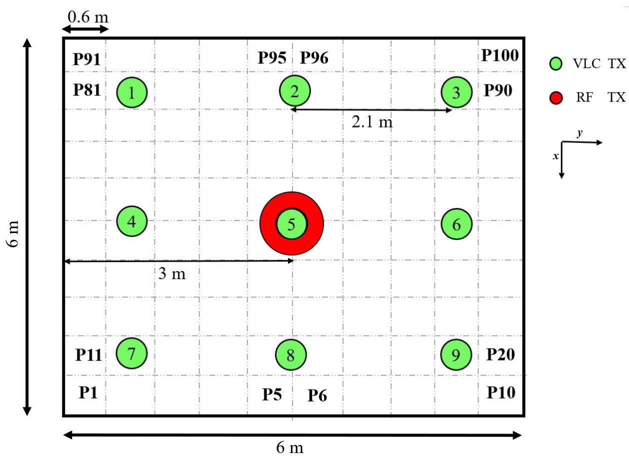

FIGURE 2. RF and VLC indoor system under consideration.

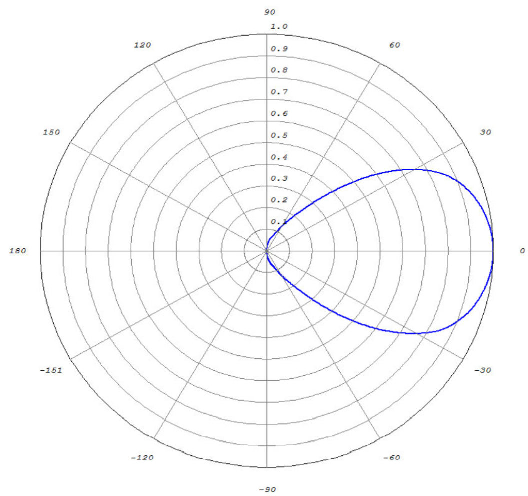

FIGURE 3. Emission pattern of each luminaire.

where H_{VLC} is the DC channel gain at the k^{th} PD. The PD converts the incident optical field into a photocurrent which is then processed electronically. Electronic processing is modeled as a trans-impedance amplifier that presents a load of R_L ohms to the photodetector. Mathematically speaking, the received electrical power is given by

$$P_{r,k} = G_A(\Re P_{r,\text{opt}})^2 R_L, \tag{7}$$

where G_A is the trans-impedance gain and $\Re$ denotes the responsivity of the PD. Replacing $P_{r,\text{opt}}$ in (10), we obtain

$$P_{r,k} = G_A(\Re \eta P_t H_k)^2 R_L, \tag{8}$$

where P_t is the transmit electrical power that drives the LED in VLC system and is related to $P_{t,\text{opt}}$ by an electrical-to-optical conversion ratio of η (i.e., $P_{t,\text{opt}} = \eta P_t$). The electrical path loss at the k^{th} PD can be finally obtained by

$$P_{\text{VLC},k} = -10\log_{10}(\frac{P_{r,k}}{P_t}). \tag{9}$$

III. INDOOR SCENARIOS

Our simulation environment is an empty room with a size of $6m \times 6m \times 3$m shown in Fig. 2. We consider 100 cells with an equidistant spacing of 0.6 m in x and y directions to investigate the effects of user locations as well as the effect of antenna locations. A user holding a phone in his hand next to his ear with 45° rotation upward to the ceiling with a height of 1.8 m is modeled. The cell phone has the size of 5.5 cm × 10.5 cm × 0.5 cm [36]. We also consider a PD with an aperture size of 1 cm^2 and an FoV of 85°. Following [36], LEDs (Cree® CR6-800L) with 40° half viewing angle are used as indoor VLC luminaires.

Fig. 3 illustrates the radiation pattern of the LED luminaire under consideration. The radiation patterns of the RF antennas are illustrated in Fig. 4, which include (a) omnidirectional antenna, (b) directional horn antenna, and (c) patched antenna. Horn antenna and rectangular patch antenna have

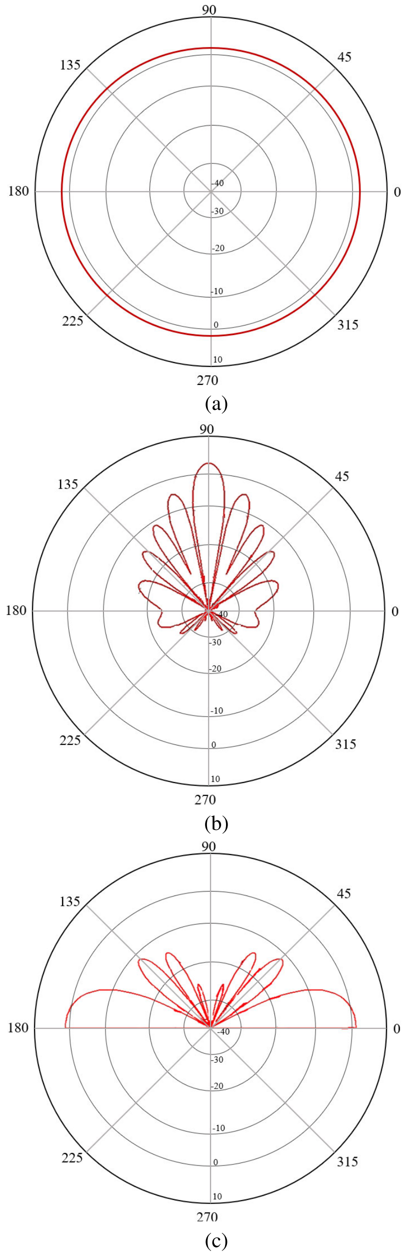

FIGURE 4. Radiation patterns: (a) isotropic omnidirectional antenna, (b) directional antenna, (c) rectangular patch antenna.

a simple structure, directional performance, high gain, wide bandwidth, and peak power handling capability. The last two advantages come from the fact that horn antennas do not have resonant elements. To have a fair comparison with VLC, we consider pyramid horn and rectangular patch antennas with a peak gain of 1 dBi and the same area of VLC receivers (i.e., 1 cm^2). These antennas are used in a beam alignment procedure in which RX orients its antenna to the direction for receiving the most powerful signal. The calculation for finding the feed/aperture sizes of the horn antenna parameters is based on [38] and [39]. In our simulation, the coating materials for walls, the ceiling, the floor, the cell phone,

TABLE 2. Material characteristics at different frequencies.

Material		Concrete	Wood	Metal	Skin
Relative permittivity (ϵ_r)		5.31	1.99	0.98	10.5
Conductivity (σ)	2.4 GHz	0.0662	0.012	3.88	1.56
	6 GHz	0.123	0.027	3.02	3.95
	28 GHz	0.48	0.167	1.98	5.32
	60 GHz	0.89	0.378	1.28	7.32
	100 GHz	1.05	0.46	0.58	9.01

TABLE 3. Simulation parameters for room and transceivers.

Parameters	Wireless Insite (RF)	OpticStudio (VLC)
Room Size	6 m× 6m× 6m	
Room surface material	Wall: Concrete Floor: Pine Wood	
Scattering / Cross polarization Factors	Lambertian R2(0.5-0.5) (Mixed diffuse and specular)	
Objects specifications	Cell Phone: Metal (Black gloss paint) Human: Face Skin and Absorbing	
No of TX	1	9
Antenna type	Omnidirectional / Directional/ Rectangular Patch	Indoor Luminaries (Lambertian)
Total Transmit Power	12 W	
Operating frequency	2.4 GHz, 6 GHz, 28 GHz, 60 GHz, 100 GHz	VLC (400–700 THz)
No of Reflections	6	
Channel Model	Ray Tracing	
No of RXs	5	
Area of RX	1 cm^2	
FoV Angle	90°	

and the human are considered as concrete drywall, wood, black glossy metal, and absorbing skin. The frequency dependence of material features can be characterized in terms of permittivity and conductivity. Table 2 presents the relative permittivity and conductivity of different materials. Table 3 provides the whole simulation parameters of both simulators including the antenna pattern and emission pattern of each LED. We consider the unit gain for all results including path loss and received power.

As shown in Fig. 5, we consider various scenarios to investigate the RF and VLC propagation channels. For the VLC system, 9 LEDs located on the ceiling act as wireless transmitters (drawn by the green circles on the ceiling in Fig. 2 and denoted by VLC TX in legend) while a single antenna represents the RF transmitter (drawn by the red circles on the ceiling in Fig. 2 and denoted by RF TX in legend). The cell phone is equipped with five receiver units denoted by RX1-RX5 as shown in Fig. 6. The RXs are distributed around the cell phone in a way to cover all possible directions where the rays can come from either directly or via reflection. To develop various snapshots of indoor communication in a room, six different scenarios are considered for the user by

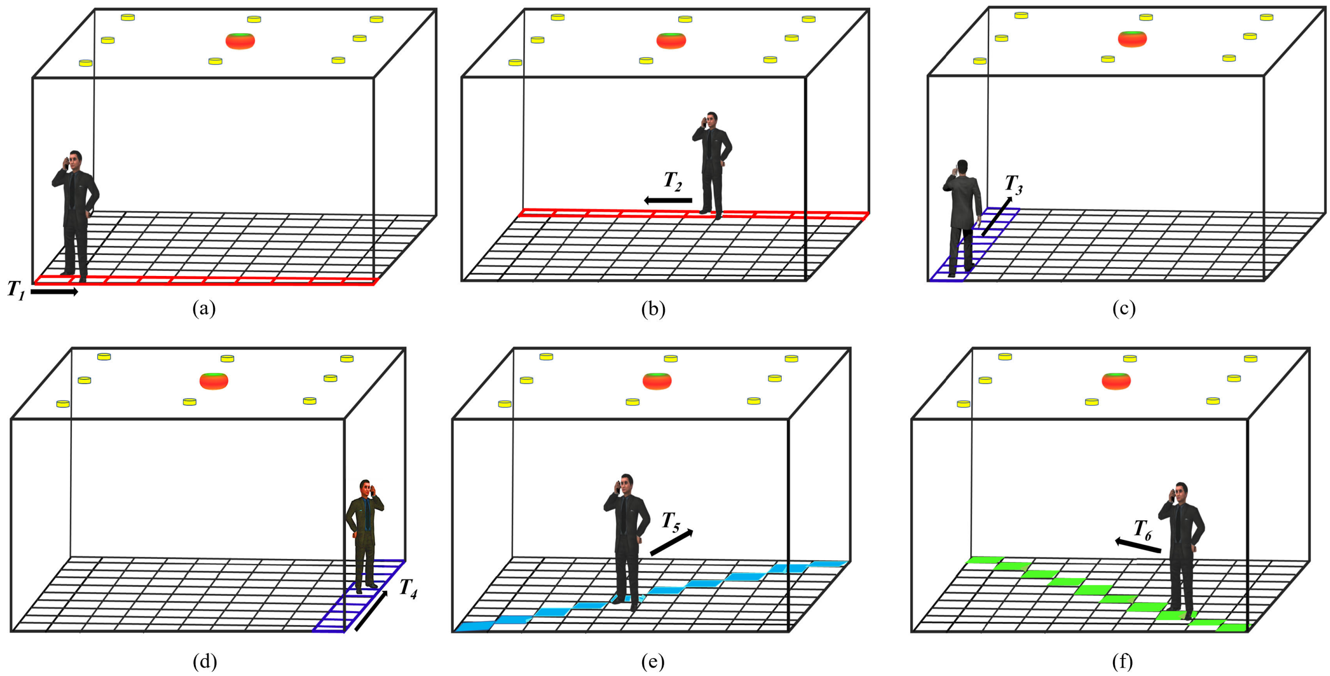

FIGURE 5. Indoor RF/VLC Scenarios, (a) Cells of T_1 related to Scenario 1, (b) Cells of T_2 related to Scenario 2, (c) Cells of T_3 related to Scenario 3, (d) Cells of T_4 related to Scenarios 4, (e) Cells of T_5 related to Scenario 5, (f) Cells of T_6 related to Scenario 6.

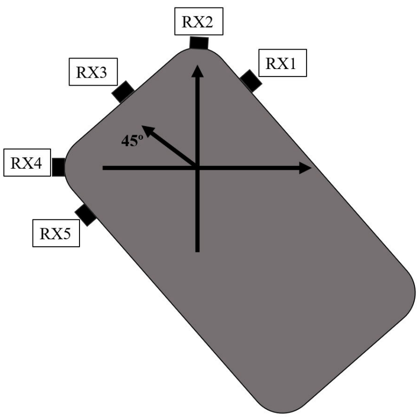

FIGURE 6. Orientation of RXs on the cell phone.

moving through trajectories (denoted by T_1, T_2,..., T_6) as detailed below:

- **Scenario 1 (Fig. 5a):** In this scenario, we consider all cells in T_1 which the user moves horizontally from the left to the right side of the room marked by the red rectangular in Fig. 5a. The cell phone is in the right hand of the user and it is directed to the inner room side.
- **Scenario 2 (Fig. 5b):** This scenario considers the cells near the north wall of our room as T_2 shown by the red rectangular in Fig. 5b. The user holds the cell phone in his right hand and changes his location from right to the left side of the room. The cell phone is directed to the wall.
- **Scenario 3 (Fig. 5c):** In this scenario, the human walks vertically from down to up near the west wall of the room to get the results of all cells in T_3, shown by the blue rectangular in Fig. 5c. The cell phone is located in the right hand of the user looking wall and completely covered by the head of the human and the wall.
- **Scenario 4 (Fig. 5d):** In this scenario, all cells of T_4 are captured from down to up near the east wall of the room to investigate the results of all antennas in the cell phone (See blue rectangular in Fig. 5d). The cell phone is directed the inner side of the room.
- **Scenario 5 (Fig. 5e):** The light blue cells located on the diagonal of Fig. 5e illustrate T_5. The user moves from one corner to the opposite one diagonally by holding the cell phone in his right hand.
- **Scenario 6 (Fig. 5f):** The light green colours in Fig. 5f denotes cells of T_6. Through this trajectory, the human holds his cell phone near his ear and changes his position from the right-south corner up to the left-north side.

IV. SIMULATION RESULTS AND DISCUSSIONS

In this section, we present simulation results for VLC and RF channels of indoor scenarios described in the previous section.

In Fig. 7, the path loss results are provided for RX1, RX2, and RX5 at 60 GHz and VLC. It is observed that the diagonal trajectories (i.e., T_5 and T_6) related to Scenarios 5 and 6 have the minimum path loss for RX1 and RX2 at the middle position of each trajectory in MMW. This trend is the same as VLC for RX2 T_3, T_5, and T_6 have lower path loss in comparison with the other trajectories. The path loss results of T_1, T_2, T_5, and T_6 significantly decrease over their initial

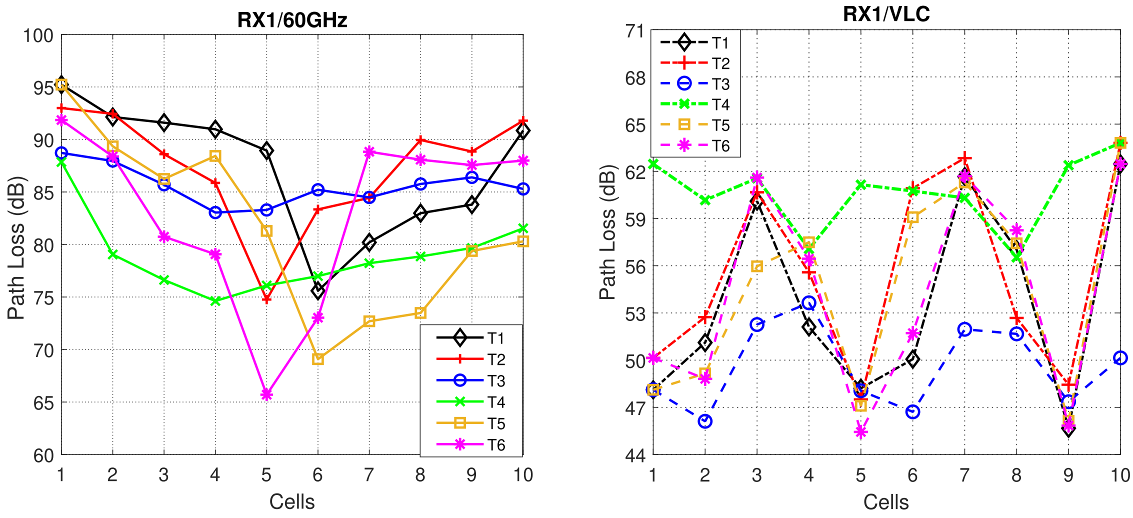

(a)

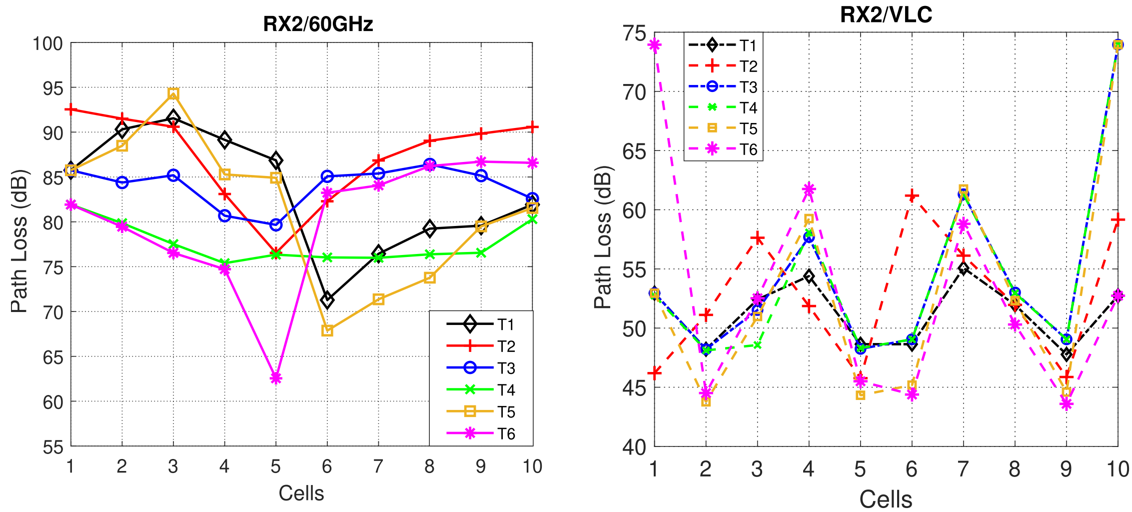

(b)

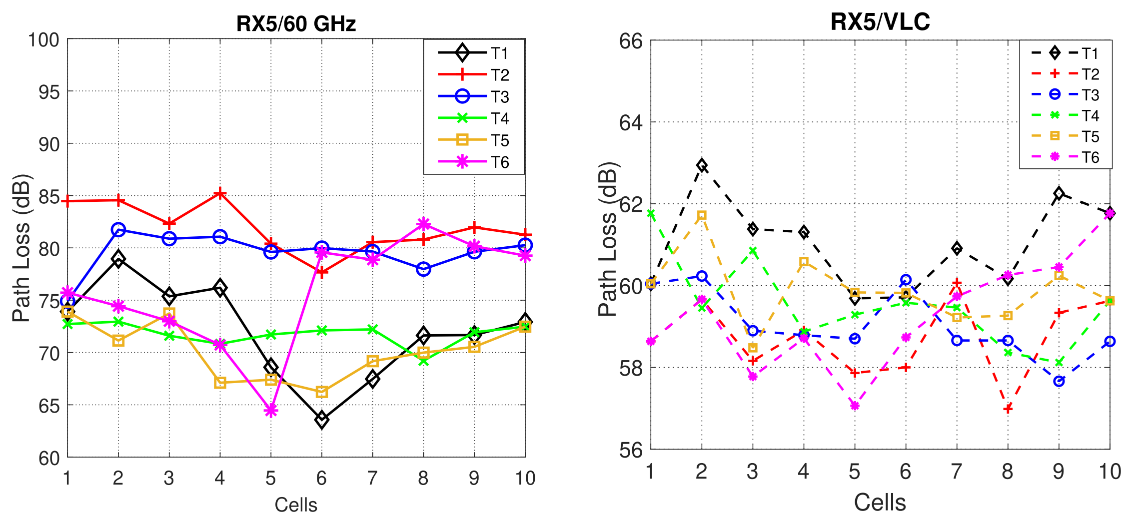

(c)

FIGURE 7. Effect of different trajectories on the path loss results for both MMW and VLC (Scenarios 1-6), considering (a) RX1, (b) RX2, and (c) RX5.

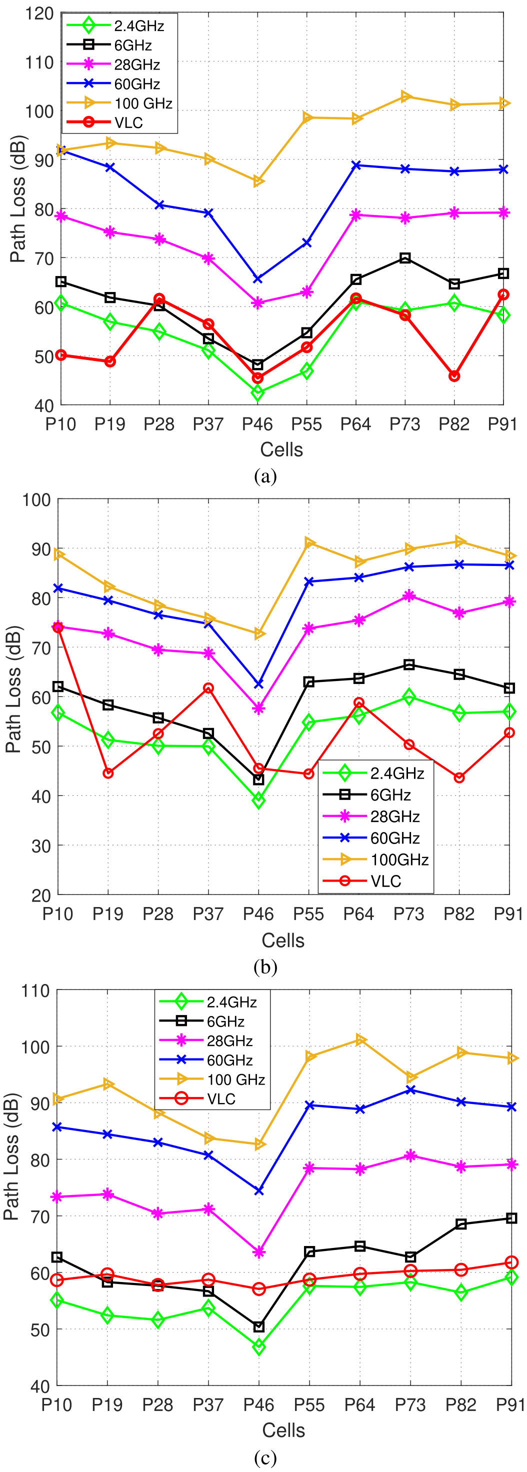

FIGURE 8. Effect of different frequencies on the path loss results considering T_6 (a) RX1, (b) RX2, and (c) RX5.

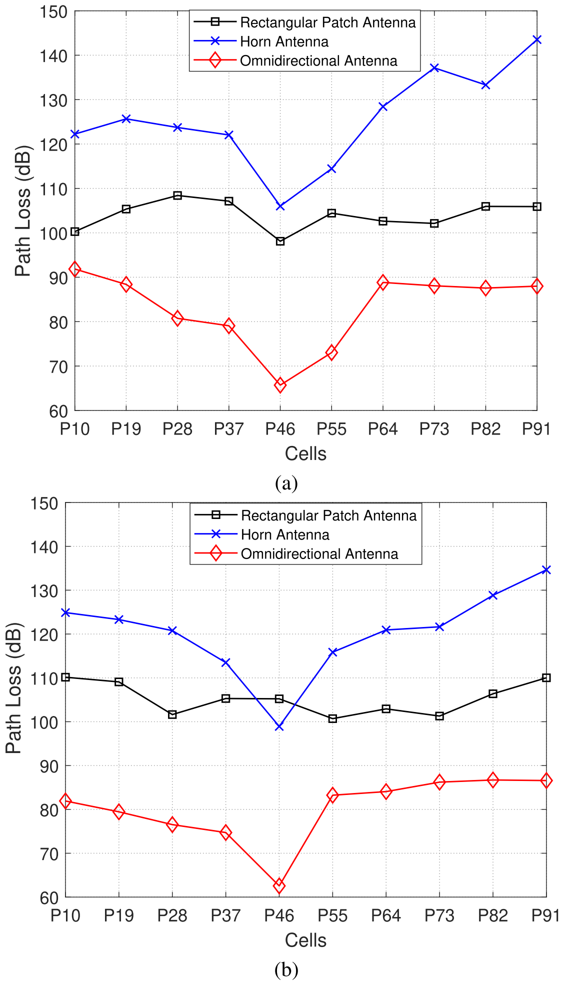

FIGURE 9. Effect of antenna type on the path loss results considering 60 GHz and trajectory T_6 for (a) RX1 and (b) RX2.

positions on the path for given MMW RXs. Having passed the middle point of those trajectories, the path loss results of T_6 witness a dramatic increase. There are upward trends in the path loss results of T_1, T_2, and T_5 but not as much as T_6. The main factor behind this is the blockage of the cell phone with the human head, which appears after passing the middle position of T_6. For T_3 and T_4, there are only slight changes.

In VLC, all trajectories experience the sinusoidal signal behaviors by RX1 and RX2 which means that there are increasing and decreasing while the user is getting away or near the LEDs on the ceiling (See Fig. 2). For RX5, the minimum path loss results are related to T_1, T_6, and T_5, respectively. Because of the location of RX5 in the cell phone (See Fig. 6), most of the received rays are 1 or 2-order reflections from the floor. The path loss of RX5 fluctuates for the initial positions of T_1 and T_5 till the middle position levelled off. Then there is a steady growth in path loss results for the last positions of T_1. By contrast, the path loss results of T_3 and T_4 are flat and there is a significant difference between those amounts due to blockage of the receivers by the head of the human and sidewall over the T_3. The maximum results of the path loss are related to T_2 where RX5 is completely covered by the human body and sidewall throughout this path. It is worth noting that again the maximum difference between the first and last positions is related to T_6. In VLC more of trajectories experience fluctuation trends.

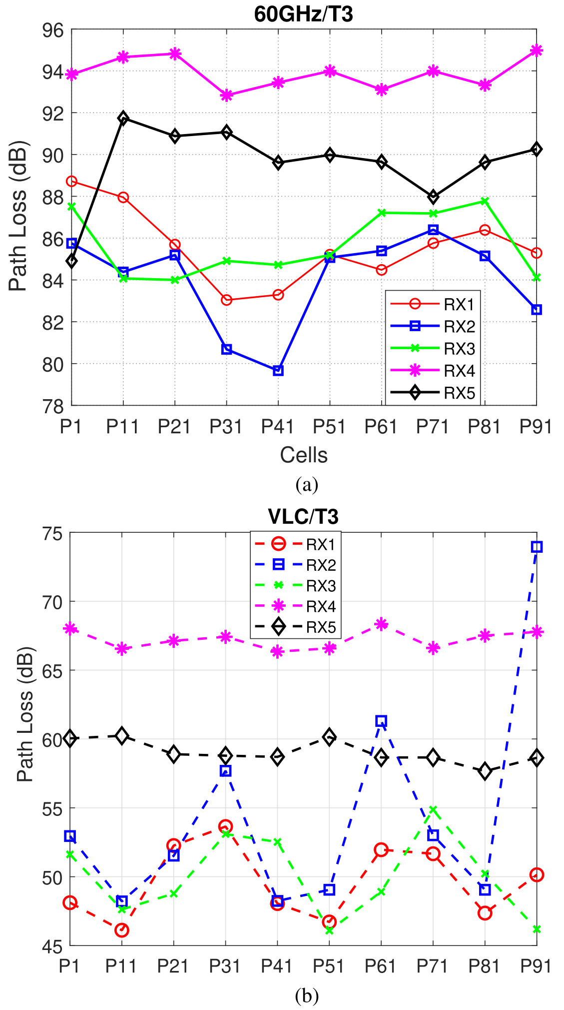

FIGURE 10. Effect of receiver locations on the path loss results of MMW and VLC considering trajectory T_3.

TABLE 4. Gaussian coefficients in the CDF functions of received powers for 2.4 GHz.

	$F_{1X}(x) = a_1 \exp\left(-\left((x-b_1)/c_1\right)^2\right)$		
2.4 GHz	a_1	b_1	c_1
RX1	0.96	2.56	14.66
RX2	1.22	4.35	16.35
RX3	1.16	1.73	16.13
RX4	0.98	4.83	11.54
RX5	1.58	3.32	12.75

TABLE 5. Gaussian coefficients in the CDF functions of received powers for 6 GHz.

	$F_{1X}(x) = a_1 \exp\left(-\left((x-b_1)/c_1\right)^2\right)$		
6.0 GHz	a_1	b_1	c_1
RX1	0.96	10.55	14.44
RX2	1.07	10.60	21.37
RX3	1.02	10.41	14.24
RX4	0.98	11.75	11.47
RX5	0.99	14.18	16.10

TABLE 6. Gaussian coefficients in the CDF functions of received powers for 28 GHz.

	$F_{1X}(x) = a_1 \exp\left(-\left((x-b_1)/c_1\right)^2\right)$		
28 GHz	a_1	b_1	c_1
RX1	0.9569	24.09	14.57
RX2	1.441	22.64	19.71
RX3	0.983	23.8	15.75
RX4	0.980	26.71	12.61
RX5	0.97	27.45	15.96

In Fig. 8, the impact of different frequencies on path loss results is presented for Scenario 6 (i.e., trajectory T_6), using omnidirectional antennas for RX1, RX2, and RX5. The results show that increasing frequency leads to an increase in path loss for all RXs. Interestingly, the results of VLC intersect with those of RF for all RXs. For instance, for RX2 (Fig. 8b), at certain positions such as P10, P37, and P64, the path loss of the 6GHz band is lower than that of the VLC band, while at other positions such as P19, P55, and P92, the opposite is true. Notably, the 2.4GHz, 6GHz, and VLC bands yield the lowest path loss results compared to higher RF bands such as 28GHz, 60GHz, and 100GHz.

Fig. 9 illustrates the effect of different antenna types on the path loss of Scenario 6 by considering 60 GHz. It is apparent from this figure that the path loss results for the omnidirectional antenna for RX1 are lower than the results for the rectangular patch and horn antennas. The factor behind this is the patterns of those antennas shown in Fig. 4 (a-c). The patch antenna cannot get rays from all directions as much as an omnidirectional antenna. On the other side, its coverage is not narrow as the horn antenna. It can be noted that the path loss of P46 with horn antenna is less than one equipped with the patch antenna. The reason is that the main lope of the patch antenna is not strong as the one in the horn antenna noting that both antennas have unit gain (See Fig. 4 b and c). The side lopes of the patch antenna are stronger than the main lope. Therefore, the path loss result of RX1 in P46 has the minimum amount, however, RX2 cannot have a minimum result regarding its location in the cell phone and the pattern of the antenna (See Fig. 4 and 6).

In Fig. 10, the path loss results are presented for all RXs assuming omnidirectional antennas for Scenario 3. Results illustrate that RX1, RX2, and RX3 have less path loss in all positions belonging to P41. The reason is that the human head covers the cell phone in his hand throughout this path, but the location of RX2 can help to get the power with less path loss by receiving the reflected signals from the ceiling. For VLC RX1-RX3 experiences less path loss than RX4 and RX5. Due to utilizing 9 LEDs on the ceiling there is not a minimum point, and the behaviour of the path loss follows a sinusoidal pattern.

In the following, we investigate the received power levels for all scenarios and frequency bands under consideration. We consider the cumulative distribution function (CDF) of received powers as seen by the individual receivers (i.e., RXs). This presents the probability that received power

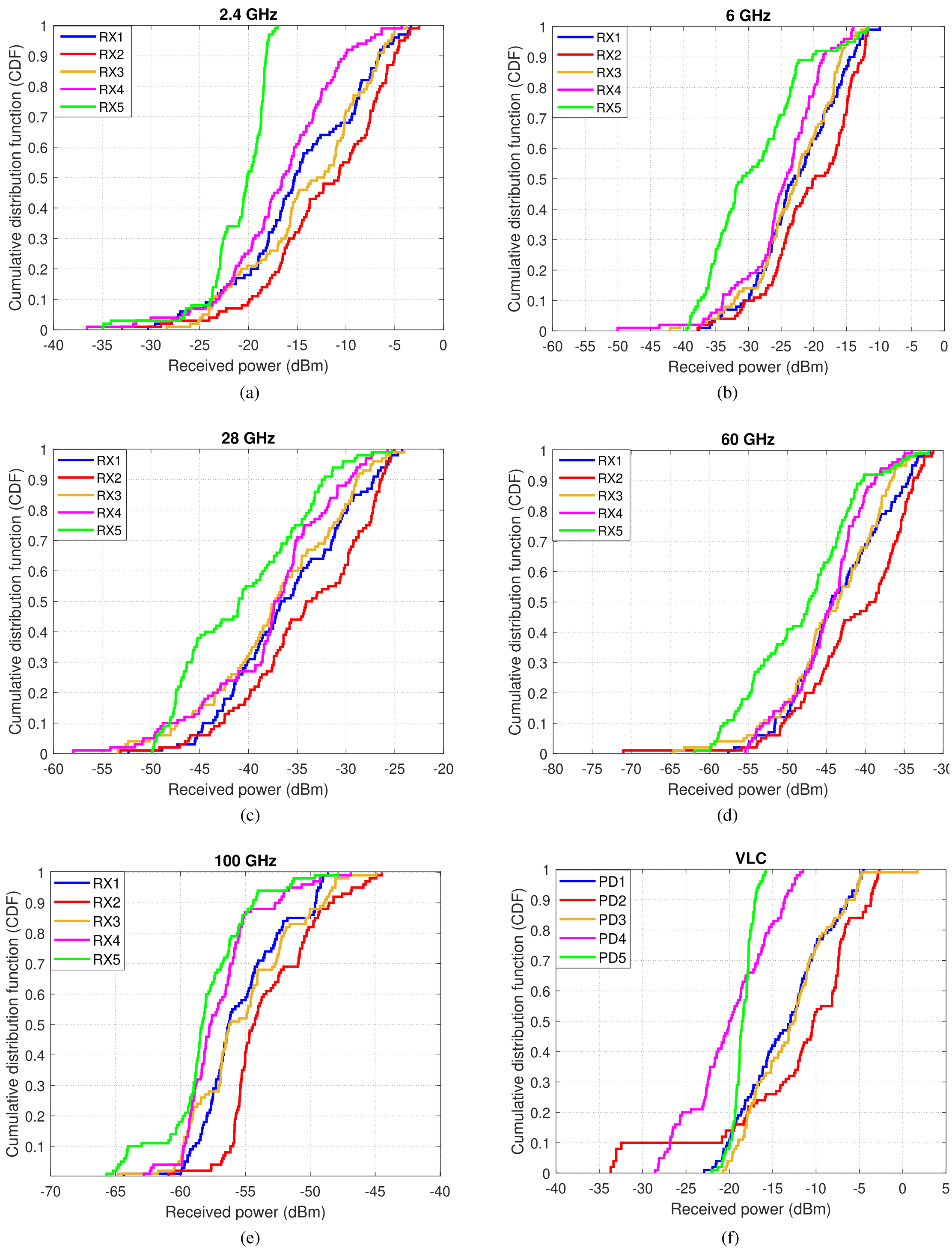

FIGURE 11. CDF of received power as seen by the individual RXs and PDs for different RF (a-e) and VLC (f) frequencies.

will take less than or equal a specific value, which is given by

$$F_X(x) = \Pr[X \leq x]. \tag{10}$$

As shown in Fig. 11, the worst case occurs for RX5 because it is located at the bottom of the cell phone and faces down (see Fig. 6). Therefore, most of the received rays at RX5 are mainly due to the first reflection from the floor or higher order reflections from the walls and ground (i.e., no LOS reception). In contrast, RX2 has the highest received power (best case) due to its ability to get LOS rays in most positions. Because it is located on the top of the cell phone and faces toward the ceiling, where TXs are located. Results also

TABLE 7. Gaussian coefficients in the CDF functions of received powers for 60 GHz.

	$F_{2X}(x) = a_1 \exp(-((x-b_1)/c_1)^2) + a_2 \exp(-((x-b_2)/c_2)^2)$					
60 GHz	a_1	b_1	c_1	a_2	b_2	c_2
RX1	0.97	29.9	3.82	0.45	31.95	10.51
RX2	0.97	37.67	3.48	1.01	30.77	12.97
RX3	0.83	39.71	3.98	1.00	34.61	11.78
RX4	1.65	31.64	4.02	1.53	29.82	16.09
RX5	0.96	32.89	2.31	0.98	33.81	16.66

TABLE 8. Gaussian coefficients in the CDF functions of received powers for 100 GHz.

	$F_{2X}(x) = a_1 \exp(-((x-b_1)/c_1)^2) + a_2 \exp(-((x-b_2)/c_2)^2)$					
100GHz	a_1	b_1		a_2	b_2	c_2
RX1	0.939	49.12	5.703	0.313	55.29	2.821
RX2	1.016	46.83	6.358	0.296	53.64	1.822
RX3	0.996	45.63	7.43	0.373	54.30	2.708
RX4	1.011	48.07	6.193	0.559	55.34	3.621
RX5	1.028	49.36	7.93	0.308	56.16	1.669

TABLE 9. Gaussian coefficients in the CDF functions of received powers for VLC.

	$F_{2X}(x) = a_1 \exp(-((x-b_1)/c_1)^2) + a_2 \exp(-((x-b_2)/c_2)^2)$					
VLC	a_1	b_1	c_1	a_2	b_2	c_2
RX1	0.096	13.63	3.38	0.89	14.37	8.71
RX2	0.12	16.61	2.96	0.668	18.93	7.22
RX3	0.300	15.41	3.24	0.877	16.94	9.16
RX4	0.255	10.58	2.98	0.807	13.61	9.10
RX5	0.099	16.23	2.43	0.80	18.38	9.84

illustrate that RX1 and RX3 have lower path loss in comparison to RX4 and RX5. Because the human head covers a part of the cell phone throughout the path, which contains RX4 and/or RX5 depending on the location. RX1 and RX3, however, experience lower path loss since they are only partially covered. In the VLC case, RX1 and RX3 can even get a LOS signal from different luminaries based on user location.

Furthermore, we propose closed-form expressions for the CDFs of indoor channels for all scenarios and receivers under consideration. We use non-linear curve fitting in the MATLAB toolbox to determine the CDF behavior of the channel path losses. At lower frequencies (i.e., 2.4 GHz, 6 GHz, and 28 GHz), the CDF of the received power is fitted with a 1-term Gaussian function. For higher frequency bands (i.e., 60 GHz, 100 GHz, and VLC), the CDF of the received power is fitted with a 2-term Gaussian function. These are given, respectively, by

$$F_{1X}(x) = a_1 \exp((-(x-b_1)/c_1)^2), \tag{11}$$

$$F_{2X}(x) = a_1 \exp((-(x-b_1)/c_1)^2) + a_2 \exp((-(x-b_2)/c_2)^2), \tag{12}$$

where, x denotes the received power (in dBm), a_1, a_2, b_1, b_2, c_1, and c_2 are coefficients of Gaussian functions with 95% confidence bounds, and adjusted R-squares of 99% provided in Table 4 - Table 9.

V. CONCLUSION

In this paper, we presented a comprehensive one-to-one comparison between indoor VLC and RF channels based on advanced ray tracing simulators. We analyzed the CIRs obtained by ray tracing and compared the path loss at different indoor scenarios and frequency bands (i.e., 2.4 GHz, 6 GHz, 28 GHz, 60 GHz, 100 GHz, and VLC band). The different antenna types (i.e., omnidirectional, directional, rectangular patch, and indoor luminaire), receiver locations, and user trajectories (i.e., diagonal, vertical, and horizontal paths) have been investigated. It has been observed that the higher the RF bands, the path loss of the channel is higher, while the VLC channels exhibit a lower path loss level than MMW bands and a higher level than 2 GHz bands. Our results further revealed that the propagation channel characteristics are highly dependent on the antenna type same as the geometry of the user and the RX. For example, using the omnidirectional and rectangular patch antennas come with lower path loss compared to the horn antennas, and such a gap significantly increases when the RX becomes closer to the TX antenna, where the direct LOS link becomes stronger. While our current study is limited to two-dimensional scenarios, three-dimensional scenarios such as vertical movement in an elevator and vertical movement of the user in the case of a spiral staircase are interesting to explore in the future.

REFERENCES

[1] T. E. Bogale and L. B. Le, "Massive MIMO and mmWave for 5G wireless HetNet: Potential benefits and challenges," *IEEE Veh. Technol. Mag.*, vol. 11, no. 1, pp. 64–75, Mar. 2016.

[2] M. Uysal, "Visible light communications: From theory to industrial standardization," in *Proc. Opt. Fiber Commun. Conf. Exhib. (OFC)*, Mar. 2019, pp. 1–3.

[3] A. Jovicic, J. Li, and T. Richardson, "Visible light communication: Opportunities, challenges and the path to market," *IEEE Commun. Mag.*, vol. 51, no. 12, pp. 26–32, Dec. 2013.

[4] Y. Chen, W. Guan, J. Li, and H. Song, "Indoor real-time 3-D visible light positioning system using fingerprinting and extreme learning machine," *IEEE Access*, vol. 8, pp. 13875–13886, 2020.

[5] P. Du, S. Zhang, C. Chen, H. Yang, W.-D. Zhong, R. Zhang, A. Alphones, and Y. Yang, "Experimental demonstration of 3D visible light positioning using received signal strength with low-complexity trilateration assisted by deep learning technique," *IEEE Access*, vol. 7, pp. 93986–93997, 2019.

[6] F. Wang, F. Yang, J. Song, and Z. Han, "Access frameworks and application scenarios for hybrid VLC and RF systems: State of the art, challenges, and trends," *IEEE Commun. Mag.*, vol. 60, no. 3, pp. 55–61, Mar. 2022.

[7] S. M. Sheikholeslami, A. Rasti-Meymandi, S. J. Seyed-Mohammadi, J. Abouei, and K. N. Plataniotis, "Communication-efficient federated learning for hybrid VLC/RF indoor systems," *IEEE Access*, vol. 10, pp. 126479–126493, 2022.

[8] H. Abuella, M. Elamassie, M. Uysal, Z. Xu, E. Serpedin, K. A. Qaraqe, and S. Ekin, "Hybrid RF/VLC systems: A comprehensive survey on network topologies, performance analyses, applications, and future directions," *IEEE Access*, vol. 9, pp. 160402–160436, 2021.

[9] A. Adnan-Qidan, M. Morales-Céspedes, and A. G. Armada, "Load balancing in hybrid VLC and RF networks based on blind interference alignment," *IEEE Access*, vol. 8, pp. 72512–72527, 2020.

[10] M. G. Sanchez, *Millimeter-Wave (mmWave) Communications*. Basel, Switzerland: MDPI-Multidisciplinary Digital Publishing Institute, 2020.

[11] S. Althunibat, R. Mesleh, and K. Qaraqe, "Secure index-modulation based hybrid free space optical and millimeter wave links," *IEEE Trans. Veh. Technol.*, vol. 69, no. 6, pp. 6325–6332, Jun. 2020.

[12] S. Kaddouri, M. E. Hajj, G. Zaharia, and G. E. Zein, "Indoor path loss measurements and modeling in an open-space office at 2.4 GHz and 5.8 GHz in the presence of people," in *Proc. IEEE 29th Annu. Int. Symp. Pers., Indoor Mobile Radio Commun. (PIMRC)*, Sep. 2018, pp. 1–7.

[13] B. M. Donlan, D. R. McKinstry, and R. M. Buehrer, "The UWB indoor channel: Large and small scale modeling," *IEEE Trans. Wireless Commun.*, vol. 5, no. 10, pp. 2863–2873, Oct. 2006.

[14] I. D. S. Batalha, A. V. R. Lopes, J. P. L. Araújo, B. L. S. Castro, F. J. B. Barros, G. P. D. S. Cavalcante, and E. G. Pelaes, "Indoor corridor and office propagation measurements and channel models at 8, 9, 10 and 11 GHz," *IEEE Access*, vol. 7, pp. 55005–55021, 2019.

[15] N. Zhang, J. Dou, L. Tian, X. Yuan, X. Yang, S. Mei, and H. Wang, "Dynamic channel modeling for an indoor scenario at 23.5 GHz," *IEEE Access*, vol. 3, pp. 2950–2958, 2015.

[16] A. G. Sreedevi, T. R. Rao, and M. Susila, "Measurements at 2.4, 3.4, 5.2, 28 and 60 GHz for device-to-device wireless communications," *Wireless Pers. Commun.*, vol. 108, no. 3, pp. 1733–1743, May 2019.

[17] Y. Xing, T. S. Rappaport, and A. Ghosh, "Millimeter wave and sub-THz indoor radio propagation channel measurements, models, and comparisons in an office environment," *IEEE Commun. Lett.*, vol. 25, no. 10, pp. 3151–3155, Oct. 2021.

[18] M. R. Prieto, R. Hofman, M. G. Sánchez, Ì. Cuíñas, I. E. Pérez, and J. Verhaevert, "Effect of space diversity for fading mitigation at 40 and 60 GHz indoor channels," in *Proc. 16th Eur. Conf. Antennas Propag. (EuCAP)*, Mar. 2022, pp. 1–5.

[19] K. Lee, H. Park, and J. R. Barry, "Indoor channel characteristics for visible light communications," *IEEE Commun. Lett.*, vol. 15, no. 2, pp. 217–219, Feb. 2011.

[20] X. Nan, P. Wang, L. Guo, L. Huang, and Z. Liu, "A novel VLC channel model based on beam steering considering the impact of obstacle," *IEEE Commun. Lett.*, vol. 23, no. 6, pp. 1003–1007, Jun. 2019.

[21] R. Raj, S. Jaiswal, and A. Dixit, "On the effect of multipath reflections in indoor visible light communication links: Channel characterization and BER analysis," *IEEE Access*, vol. 8, pp. 190620–190636, 2020.

[22] F. Miramirkhani and M. Uysal, "Channel modeling and characterization for visible light communications," *IEEE Photon. J.*, vol. 7, no. 6, pp. 1–16, Dec. 2015.

[23] Z. N. Chaleshtori, Z. Ghassemlooy, H. B. Eldeeb, M. Uysal, and S. Zvanovec, "Utilization of an OLED-based VLC system in office, corridor, and semi-open corridor environments," *Sensors*, vol. 20, no. 23, p. 6869, Dec. 2020.

[24] S. M. Nlom, A. R. Ndjiongue, and K. Ouahada, "Cascaded PLC-VLC channel: An indoor measurements campaign," *IEEE Access*, vol. 6, pp. 25230–25239, 2018.

[25] H. B. Eldeeb, S. M. Mana, V. Jungnickel, P. Hellwig, J. Hilt, and M. Uysal, "Distributed MIMO for Li-Fi: Channel measurements, ray tracing and throughput analysis," *IEEE Photon. Technol. Lett.*, vol. 33, no. 16, pp. 916–919, Aug. 15, 2021.

[26] S. Yahia, Y. Meraihi, A. Ramdane-Cherif, A. B. Gabis, D. Acheli, and H. Guan, "A survey of channel modeling techniques for visible light communications," *J. Netw. Comput. Appl.*, vol. 194, pp. 1–31, Sep. 2021.

[27] L. Feng, H. Yang, R. Q. Hu, and J. Wang, "MmWave and VLC-based indoor channel models in 5G wireless networks," *IEEE Wireless Commun.*, vol. 25, no. 5, pp. 70–77, Oct. 2018.

[28] I. Stefan, H. Burchardt, and H. Haas, "Area spectral efficiency performance comparison between VLC and RF femtocell networks," in *Proc. IEEE Int. Conf. Commun. (ICC)*, Jun. 2013, pp. 3825–3829.

[29] *Wireless Insite*. Accessed: Dec. 30, 2022. [Online]. Available: http://www.remcom.com/wireless-insite/

[30] *Zemax, OpticStudio*. Accessed: Dec. 30, 2022. [Online]. Available: https://www.zemax.com/pages/opticstudio

[31] T. K. Geok, F. Hossain, and A. T. W. Chiat, "A novel 3D ray launching technique for radio propagation prediction in indoor environments," *PLoS ONE*, vol. 13, no. 8, Aug. 2018, Art. no. e0201905.

[32] J. Zhang, J. Lin, P. Tang, W. Fan, Z. Yuan, X. Liu, H. Xu, Y. Lyu, L. Tian, and P. Zhang, "Deterministic ray tracing: A promising approach to thz channel modeling in 6G deployment scenarios," *IEEE Commun. Mag.*, 2023.

[33] T. K. Geok, F. Hossain, S. K. A. Rahim, O. Elijah, A. A. Eteng, C. T. Loh, L. L. Li, C. P. Tso, T. A. Rahman, and M. N. Hindia, "3D RT adaptive path sensing method: RSSI modelling validation at 4.5 GHz, 28 GHz, and 38 GHz," *Alexandria Eng. J.*, vol. 61, no. 12, pp. 11041–11061, Dec. 2022.

[34] H. B. Eldeeb, M. Uysal, S. M. Mana, P. Hellwig, J. Hilt, and V. Jungnickel, "Channel modelling for light communications: Validation of ray tracing by measurements," in *Proc. 12th Int. Symp. Commun. Syst., Netw. Digit. Signal Process. (CSNDSP)*, Jul. 2020, pp. 1–6.

[35] A. Uyrus and B. Turan, *Effects of Building Materials and Structures on Radio Wave Propagation Above About 100 MHz*, document Rec. ITU-R P.2040-1, Jul. 2015, vol. 1.

[36] M. Uysal, F. Miramirkhani, T. Baykas, and K. Qaraqe, *IEEE 802.11bb Reference Channel Models for Indoor Environments*, document IEEE 11-18-1582-02-00bb, IEEE P802.11 Wireless LANs, Sep. 2018. Accessed: Aug. 7, 2023. [Online]. Available: https://mentor.ieee.org/802.11/dcn/18/11-18-1582-0000bb-ieee-802-11bb-reference-channel-models-for-indoor-environments.pdf

[37] H. Ling, R.-C. Chou, and S.-W. Lee, "Shooting and bouncing rays: Calculating the RCS of an arbitrarily shaped cavity," *IEEE Trans. Antennas Propag.*, vol. 37, no. 2, pp. 194–205, Feb. 1989.

[38] G. Abhignya, B. Yogita, C. Abhinay, and B. Balaji, "Design, fabrication, and testing of pyramidal horn antenna," *Int. J. Eng. Appl. Sci.*, vol. 2, no. 24, pp. 2394–3661, Apr. 2015.

[39] *Wr-15 Waveguide Standard Gain Horn Antenna Operating From 50 GHz to 75 GHz With a Nominal 25 dBi Gain With UG-385/U-Mod Round Cover Flange*. Accessed: Dec. 30, 2022. [Online]. Available: https://www.pasternack.com/wr-15-waveguide-gain-horn-antenna-25dbi-ug-385-mod-round-flange-/pewan1012-p.aspx

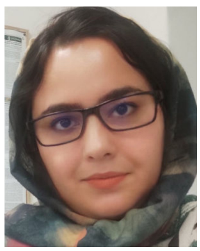

FAHIMEH AGHAEI (Student Member, IEEE) received the B.Sc. degree in electronics and electrical communication engineering from Isfahan University, in 2011, and the M.Sc. degree in electronics and electrical communication engineering from Islamic Azad University, Najafabad Branch, in 2015. She is currently pursuing the Ph.D. degree in electrical and electronics engineering with Özyeğin University, Istanbul, Turkey. Her research interests include 5G/6G wireless communication, ray tracing channel modeling, reconfigurable intelligent surface (RIS) assisted communication systems, and vehicular communication.

HOSSIEN B. ELDEEB (Senior Member, IEEE) received the M.Sc. degree in electrical and electronics engineering from Cairo University, Giza, Egypt, in 2018, and the Ph.D. degree in electrical and electronics engineering from Özyeğin University, Istanbul, Turkey, in 2021. He is currently a Research Fellow with the Electrical Engineering and Computer Science Department, Khalifa University, Abu Dhabi, United Arab Emirates. He has authored more than 35 publications in prestigious journals, conferences, and standards, and his research has been cited more than 500 times, with an H-index of 15. His research interests include 5G/6G communications, optical wireless communications, vehicular networks, AI/ML for security and signal processing, reconfigurable intelligent surfaces, and physical layer security. He received the Best Student Paper Award from IEEE/IET CSNDSP 2020 and the Best Presentation Award from GITW 2022. He was a member of the technical program committee of a number of IEEE conferences, such as CyberSciTech/PICom/DASC/CBDCom, VTC, ITC, and ATC. Additionally, he has a contribution to the IEEE standardization on VLC.

LINA BARIAH (Senior Member, IEEE) received the M.Sc. and Ph.D. degrees in communications engineering from Khalifa University, Abu Dhabi, United Arab Emirates, in 2015 and 2018, respectively. She was a Visiting Researcher with the Department of Systems and Computer Engineering, Carleton University, Ottawa, ON, Canada, in 2019, and a Research Fellow with the James Watt School of Engineering, University of Glasgow, U.K. She is currently a Senior Researcher with the Technology Innovation Institute, an Adjunct Faculty with Khalifa University, and an Adjunct Research Professor with Western University, Canada. Her research interests include machine learning for wireless communications, large language models, and generative AI for telecom. She is a Senior Member of the IEEE Communications Society, IEEE Vehicular Technology Society, and IEEE Women in Engineering. She was a member of the technical program committee of a number of IEEE conferences, such as ICC and Globecom. She serves as the Session Chair and an active reviewer for numerous IEEE conferences and journals. She has organized several workshops/special sessions in IEEE flagship conferences, including IEEE VTC and IEEE ICC. She is an Associate Editor of the IEEE Communications Letters and the IEEE Open Journal of the Communications Society. She is an Area Editor of *Physical Communication* (Elsevier). She is a Guest Editor of *IEEE Communications Magazine*, *IEEE Network Magazine*, and IEEE Open Journal of Vehicular Technology.

SAMI MUHAIDAT (Senior Member, IEEE) received the Ph.D. degree in electrical and computer engineering from the University of Waterloo, Waterloo, ON, Canada, in 2006. From 2007 to 2008, he was an NSERC Postdoctoral Fellow with the Department of Electrical and Computer Engineering, University of Toronto, Canada. From 2008 to 2012, he was an Assistant Professor with the School of Engineering Science, Simon Fraser University, BC, Canada. He is currently a Professor with Khalifa University and an Adjunct Professor with Carleton University, Ottawa, ON, Canada. His research interests include advanced digital signal processing techniques for wireless communications, intelligent surfaces, MIMO, optical communications, massive multiple access techniques, backscatter communications, and machine learning for communications. He is an Area Editor of the IEEE Transactions on Communications, a Guest Editor of the IEEE Network Special Issue on "Native Artificial Intelligence in Integrated Terrestrial and Non-Terrestrial Networks in 6G", and the IEEE Open Journal of Vehicular Technology Special Issue on "Recent Advances in Security and Privacy for 6G Networks". He served as a Senior Editor and an Editor for the IEEE Communications Letters, an Editor for the IEEE Transactions on Communications, and an Associate Editor for the IEEE Transactions on Vehicular Technology.

MURAT UYSAL (Fellow, IEEE) received the B.Sc. and M.Sc. degrees in electronics and communication engineering from Istanbul Technical University, Istanbul, Turkey, in 1995 and 1998, respectively, and the Ph.D. degree in electrical engineering from Texas A&M University, College Station, TX, USA, in 2001.

He began his academic career as an Assistant Professor with the University of Waterloo, Canada, in 2002, and was promoted to an Associate Professor with tenure, in 2007. In 2011, he joined Özyeğin University, Turkey, where he served as the Department Chair of the Electrical and Electronics Engineering and the Founding Director of the Center of Excellence, Optical Wireless Communication Technologies (OKATEM). In September 2023, he joined New York University Abu Dhabi, as a Professor of electrical engineering with tenure. His research interests include communication theory with a particular emphasis on the physical layer aspects of wireless communication systems in radio and optical frequency bands. On these topics, he has authored some 400 journal and conference papers and received more than 20,000 citations with an H-index of 63.

Dr. Uysal's major distinctions, including the NSERC Discovery Accelerator Award, in 2008; the University of Waterloo Engineering Research Excellence Award, in 2010; the Turkish Academy of Sciences Distinguished Young Scientist Award, in 2011; the Özyeğin University Outstanding Researcher Award, in 2014; the National Instruments Engineering Impact Award, in 2017; the Elginkan Foundation Technology Award, in 2018; the IEEE Communications Society Best Survey Paper Award, in 2019; and the IEEE Turkey Section Outstanding Service Award, in 2021. He is the former Chair of the IEEE Turkey Section. He was involved in the organization of several IEEE conferences at various levels. In particular, he served as the Technical Program Committee Chair for major IEEE conferences, including WCNC 2014, PIMRC 2019, and VTC-Fall 2019. From 2011 to 2015, he was the Chair of the EU COST Action OPTICWISE, a high-profile consolidated European scientific platform which brought together more than 150 researchers in the research area of optical wireless communication. He serves as an Area Editor for IEEE Transactions on Communications. In past, he served as an Editor for IEEE Transactions on Communications, IEEE Transactions on Wireless Communications, IEEE Transactions on Vehicular Technology, and IEEE Communications Letters.